Trends in Peptide and Protein Sciences
Volume 8 (2023): e4

DOI: https://doi.org/10.22037/tpps.v8i1.41609

Original Article

Synthesis and Characterization of Amyloid Beta-Lactoglobulin-Mumijo-Nanohydroxyapatite Complex: A New Composite for Bone Regeneration

Negar Khiabani[a], Azadeh Hekmat[a,*] and Aghdas Banaei[b]

[a] *Department of Biology, Science and Research Branch, Islamic Azad University, Tehran, Iran.*
[b] *Department of Biology, Research Institute of Applied Science, Academic Center of Education, Culture and Research (ACECR), Tehran, Iran.*

Article history:
Received: 16 March 2023
Accepted: 11 July 2023

Keywords:
Beta-lactoglobulin
Bone fractures
Fibrillar protein
Mumijo
Nano-sized hydroxyapatite

Negar Khiabani:
https://orcid.org/0009-0002-0978-2953

Azadeh Hekmat:
https://orcid.org/0000-0003-0123-1575

**Corresponding Author:*
Email: hekmat@ut.ac.ir (A. Hekmat)

HIGHLIGHTS

- The fibrillar BLG-Mumijo-nHA complex was synthesized in detail.
- UV-Visible, fluorescence emission, and CD spectroscopy as well as ζ-potential value confirmed the formation of a complex.
- The complex could be a good candidate for tissue engineering.

ABSTRACT

Mumijo is a traditional drug that has been used in traditional medicine for a long time and its aqueous extract is used for the treatment of osteoporosis and bone fractures. Besides, in modern medicine, nano-sized hydroxyapatite (nHA) has achieved immense attention for bone integration and regeneration of bony defects treatment. Since the frequency of accidental bone disorders and damage is growing worldwide, the need for artificial bone implants is increasing. Thus, in this study, the fibrillar beta-lactoglobulin (BLG)-Mumijo-nHA complex was synthesized and characterized by UV–Visible, fluorescence, Fourier transform infrared, circular dichroism spectroscopy, scanning electron microscopy, and zeta potential analysis. The results showed that the fibrillar BLG-Mumijo-nHA complex was formed. The results also confirmed that the complex had a negative surface charge and was moderately stable. Cell viability assays indicated that fibrillar BLG-Mumijo-nHA complex induced bone marrow-derived mesenchymal stem cell growth at higher concentrations. Although further experiments are warranted to draw firm conclusions, it could be proposed that the fibrillar BLG-Mumijo-nHA complex could be a good candidate for the treatment of osteoporosis and bone fractures.

Cite this article as: Khiabani, N., Hekmat, A. and A. Banaei, (2023). Synthesis and characterization of the amyloid beta-lactoglobulin-Mumijo-nanohydroxyapatite complex: A new composite for bone regeneration. *Trends Pept. Protein Sci.*, **8**: e4.

Introduction

Postnatal bone inherits the ability to renovate in response to injury or mechanical stimuli. However, any failure in this process leads to limiting the self-healing ability of the bone (Bhattacharjee et al., 2017). Consequently, it is urged to develop non-toxic and

cost-effective treatments centered on tissue engineering and regenerative medicine. Natural bone is a nano-fibril complex that contains an orderly deposition of hydroxyapatite mineral crystals formed within a collagen matrix. Hydroxyapatite is one of the most common apatites utilized as bioceramics in tissue engineering and regenerative medicine (Saxena et al., 2021). The term nanopharmaceuticals, a fundamental part of nanomedicine, includes the application of nanomaterials as therapeutic agents as well as the delivery of drugs (Hekmat et al., 2022). More recently, the nano-sized hydroxyapatite (nHA), has achieved immense attention for bone integration and regeneration of bony defects treatment. Although hydroxyapatite is a material with good bioactivity and biocompatibility, however, this material has poor mechanical properties (Saber-Samandari et al., 2016). To solve this disadvantage, several degradable natural polymers as flexible reinforcing agents have been combined with nHA to improve its mechanical properties, such as fibrin and fibrinogen (Noori et al., 2017; Meimandi-Parizi et al., 2018), collagen (Arpornmaeklong et al., 2023), silk (Bhattacharjee et al., 2017; Zhao et al., 2022), and gelatin (Meimandi-Parizi et al., 2018; Sadeghinia et al., 2019).

Milk contains a large amount of calcium and is one of the main sources of dietary calcium. Beta-lactoglobulin (BLG) is the main protein in cattle and other ruminant milk, with high nutritional value, an isoelectric point of ~ 5.13, and a molecular weight of 18.3 kDa. This globular protein has a β-barrel structure consisting of eight antiparallel β-sheets (Mohammad-Beigi et al., 2023). BLG is a mixture of monomer and dimer forms. BLG keeps its dimeric form over a wide pH range from pH 3 to pH 8, as long as a temperature over 20 °C and a moderate ionic strength (<100 mM). Nevertheless, at below pH 3 and ionic strength of <10 mM BLG is mainly monomeric (Mercadante et al., 2012). BLG could be transferred to long fibrillary amyloid aggregates by utilizing high temperature (~90 °C) at ~pH 2 and low ionic strength during an incubation time of several hours. Amyloid fibrils from BLG display invaluable functional features owing to their stiffness and high aspect ratio along with their collective ordering characteristics. Thus, amyloid fibrils have gradually been applied as new materials (Wei et al., 2017; Bolisetty et al., 2019; Cao et al., 2019). It has been shown that α-casein and BLG have antioxidant activity and could prevent skeletal muscle loss (Kim et al., 2019). Douglas *et. al.* proved that whey protein especially BLG can behave as an enhancer of osteogenic differentiation and cell proliferation (Douglas et al., 2018). Jang *et. al.* also demonstrated after the treatment of rats with a high dose of whey protein, calcium levels diminished meaningfully, whereas insulin-like growth factor-1 level, alkaline phosphatase level, growth plate height, as well as tibia length incremented considerably, i.e., whey protein has stimulant effects on bone growth and bone differentiation (Jang et al., 2021). Hence, the enrichment of biomaterials for bone regeneration with BLG seems a promising approach.

Mumijo (common names: Silajita, Shilajit, Gujarati or Marathi (in Hindi), Silajatu (in Bengali), Rock juice (in Tibet), Asphalt (in English), Moomiaii or Mumnaei (in Persian), Mumie (in German), μούμια (in Greek), Conqueror of mountains (in Sanskrit), Hajarul-Musa or Araq-al-jibal (in Arabic), Bragshun, mineral wax, jew's pitch, and mineral pitch) is a pale-brown to blackish-brown resin formed through long-term humification of numerous plant types, mostly bryophytes, present in the vicinity of shilajit-exuding rocks (Mishra et al., 2019; Ding et al., 2020; Kloskowski et al., 2021). This natural substance has been utilized for over 4000 years in traditional medicine. Regularly, Mumijo has been found as crusts in rock cracks or interstices in the Himalayas mountain, and mountainous areas in southern Kazakhstan, Nepal, Iran, Norway, Tibet, Bhutan, China, Caucasus, Pakistan, and Afghanistan. Mumijo is utilized as a remedy for injuries, dislocations, and bone fractures, skin diseases, as well as for the treatment of osteoporosis. Furthermore, Mumijo has been employed as a treatment for nervous diseases, digestive disorders, diabetes, chronic bronchitis, eczema, anemia, and tuberculosis (Mishra et al., 2019). Mumijo is soluble in water, and ~30-50% of its ingredients are moved into the liquid phase. Commonly, Mumijo is composed of organic (60-80%) and inorganic (20-40%) compounds and trace elements (P, Mo, Mn, Mg, Zn, Cu, Ca, Fe) (Mishra et al., 2019; Aiello et al., 2011). Additionally, Mumijo is a rich source of exogenous amino acids (for instance threonine, leucine, and methionine), endogenous amino acids (such as aspartic acid, tyrosine, arginine, glycine, proline, and histidine), fatty acids, and vitamins B1 and B12 (Cesur et al., 2019). More recently, researchers demonstrated the effective role of Mumijo in the treatment of osteoporosis and bone fractures (Abbasi et al., 2019; Cesur et al., 2019; Pingali et al., 2022).

Based upon the abovementioned properties of nHA and Mumijo, we hypothesized that administration of these substances with fibrillar BLG could utilize in the treatment of bone fractures. It should be noted that this is the first attempt to introduce the fibrillar BLG-Mumijo-nHA complex for bone regeneration in detail using multiple spectroscopic instruments and scanning electron microscopy (SEM). Furthermore, the impacts of the fibrillar BLG-Mumijo-nHA complex on the growth and viability of bone marrow-derived mesenchymal stem cells (rBMMSCs) were investigated.

Materials and Methods

Bovine BLG (Lyophilized powder; from bovine; ≥90% purity) and MTT (3-[4, 5-dimethylthiazol-2-yl]-2, 5-diphenyl tetrazolium bromide) were purchased from Sigma Aldrich Co., USA. The stock solution of BLG was prepared by dissolving 1 mg of BLG in 1 mL Tris buffer (pH 7.4, 0.1 M). Nano-hydroxyapatite (White powder; $Ca_{10}(PO_4)_6(OH)_2$; needle-shaped; average particle size ~30 nm; density 3.1 g/cm^3) was acquired from SPIC Petroblend Co., Iran. Mumijo (Ayurveda Shilajit Resin; semi-liquid form) was obtained from Vedapure Natural Pvt Ltd., India. Tris(hydroxymethyl)aminomethane (Tris-base), Tris(hydroxymethyl)aminomethane hydrochloride (Tris-HCl), and a 0.22 µm syringe filter were purchased from Merck Co, USA. The cell culture medium (low glucose DMEM), fetal bovine serum (FBS), Trypsin-EDTA, penicillin, and streptomycin were supplied by Gibco Co., USA.

BLG fibrillation

The fibrillar BLG solution was prepared as described by Keppler *et al.* (Keppler et al, 2019). The solution of BLG, adjusted to pH 2 (Tris-HCl, 0.1 M), was sealed with a magnetic stir-bar in heat-durable glass containers consuming plastic screw-caps and placed in a 343 K oil bath for 230 min. To avoid localized heating effects, the solution was stirred via a magnetic stir plate, located underneath the oil bath. After filtration, the exact concentration of fibrillar BLG was determined by the UV spectrum of BLG utilizing a molecular absorption coefficient of $\varepsilon_{278\,nm}$=17,600 M^{-1} cm^{-1} (Dufour et al., 1992).

Fibrillar BLG-Mumijo-nHA complex preparation

At first, 20 gr Mumijo was dissolved in 100 ml of deionized water; stirred well on a hot plate for 15 min, and centrifuged (500×g, 10 min, RT) to precipitate insoluble inorganic components. The supernatant was filtered through a 0.22 µm syringe filter. Then the stock solution of nHA was prepared by dissolving 10 mg of nHA in 2 mL Tris buffer (4.9 mM). For preparing the fibrillar BLG-Mumijo-nHA complex, the solutions of nHA and Mumijo were mixed at a ratio of 1:1. Then the solution was stirred via a magnetic stir-plate. The mixture solution was then added to the fibrillar BLG solution and stirred for 10 min.

X- ray diffraction investigation

The nHA powder was utilized to take X- ray diffraction (XRD). The XRD pattern was obtained using Cu Kα radiation of a wavelength of 0.154 nm by the XRD (Seifert 3003 T/T, Seifert, Germany). By employing equation 1 (Scherrer equation), the crystal size (D) of nHA was calculated (Saini et al., 2017). In this equation, θ, λ, and β are the scattering angle in radians, the wavelength of the X-rays in nanometer (nm), t, and the peak full width of the diffraction peak profile at half-maximum height (in radians), respectively.

$$D = \frac{0.9\lambda}{\beta \cos\theta} \qquad \text{(Eq.1)}$$

Ultraviolet-visible (UV-Vis) investigation

The UV–Vis spectra of 0.24 µM solution of BLG in pH 7.4 (native BLG), 0.24 µM solution of fibrillar BLG, 4.9 mM nHA, 0.2 g/mL Mumijo, and fibrillar BLG-Mumijo-nHA complex were recorded at 310 K in the range of 200-400 nm. All experiments were run and verified by the Varian Cary 100 Bio UV-Visible Spectrophotometer (Agilent Technologies, USA) in a 1 cm quartz cell.

Steady-state fluorescence investigation

Steady-state fluorescence emission spectra of 0.24 µM solution of native BLG, 0.24 µM solution of fibrillar BLG, 4.9 mM nHA, 0.2 g/mL Mumijo, and fibrillar BLG-Mumijo-nHA complex were explored at 310 K by the Varian Cary Eclipse Fluorescence Spectrophotometer (Agilent Technologies, USA). The thickness of the quartz cuvettes in all experiments was 1 cm and the width of the slits for excitation and emission were 10 nm and 10 nm, respectively. The fluorescence intensity spectrum for each

sample was achieved by a fluorescence cuvette with a 1 cm path length. The excitation and emission wavelengths were 280 nm and 334 nm, respectively. For inner filter effect correction caused thru the excitation and emission signals attenuation produced from the quencher absorption, equation 2 was applied (Hekmat et al., 2020).

$$F_{corr} = F_{obs}.10^{(Ab_{ex}+Ab_{em})/2} \quad \text{(Eq.2)}$$

In equation 2, F_{corr}, F_{obs}, $Ab_{ex,}$ and Ab_{em} are the corrected intensities, the observed fluorescence intensities, the mixture absorption at excitation, and the mixture absorption at emission wavelengths, respectively.

Circular dichroism (CD) investigation

The far-UV CD spectra of 0.24 µM solution of native BLG, 0.24 µM solution of fibrillar BLG, 4.9 mM nHA, 0.2 g/mL Mumijo, and fibrillar BLG-Mumijo-nHA complex were recorded from 190 to 260 nm at 310 K by the AVIV 215 Circular Dichroism Spectrometer (Aviv Biomedicals Inc., USA). The experiments were done in a quartz cell (0.1 cm path length). The resolution was 0.2 nm and the speed of scanning was 20 nm min^{-1}. By subtracting the proper baseline, each CD spectrum was corrected. The CD spectra deconvolution software (CDNN, version 2.1) was utilized to deconvolute all CD-spectra.

Fourier transform infrared (FTIR) investigation

FTIR spectra of 0.24 µM solution of native BLG, 0.24 µM solution of fibrillar BLG, 4.9 mM nHA, 0.2 g/mL Mumijo, and fibrillar BLG-Mumijo-nHA complex in the range of 400-4000 cm^{-1} were acquired by the NEXUS 870 FTIR spectrometer (Thermo Nicolet; the Thermo Fisher Scientific, USA).

Scanning electron microscope (SEM) investigation

The surface morphology of native BLG, 0.24 µM solution of fibrillar BLG, 4.9 mM nHA, 0.2 g/mL Mumijo, and fibrillar BLG-Mumijo-nHA complex were analyzed by the Zeiss DSM 960A scanning electron microscope (Carl Zeiss, Germany).

Zeta potential investigation

Zeta potential experiments were performed at SZ-100V2 Zeta-Potential (HORIBA, Ltd., Japan). Results from five experiments were averaged. Before measuring, all samples were filtered via 0.20 µm nylon filters.

Cells and cell culture

rBMMSCs were a kind gift from the Department of Tissue Engineering and Applied Cell Sciences, Tehran University of Medical Sciences (Islam et al., 2022). The cells were maintained in low glucose DMEM medium supplemented with, penicillin and streptomycin (100 U/mL) and 10% heat-inactivated FBS, in a 5% CO_2 humidified atmosphere incubator at 37 °C.

Measurement of cell viability

rBMMSCs were rinsed in DMEM and incubated with various concentrations of fibrillar BLG-Mumijo-nHA (5, 10, 20, 30, 40, 50 µL/mL). After 48 h, 25 µl of fresh MTT solution (5 mg/mL in PBS) was added to each well including fresh and cultured medium, and incubated for 3 h at 37 °C in a CO_2 incubator. Later, the insoluble formazan formed was dissolved in 100 µl of DMSO and mixed. The OD (optical density) of each well at 570 nm, was measured against a reagent blank with an ELISA reader (ELx808, BioTek Instruments, Inc., USA). Each trial was repeated 3 times.

Statistical analysis

Significant alterations were calculated by t-test of GraphPad Prism Software (Version 8.4.3, GraphPad Software Inc., San Diego, USA). All data were specified as the mean ± the standard deviation (SD) and * reveals a significant difference.

Results and Discussion

Characterization of nHA

XRD is the most practical technique for the characterization of crystalline material. Fig. 1 shows diffraction peaks of nHA at 2θ~25.92°, 31.12°, 31.76°, 32.16°, 32.88°, 39.76°, 46.80°, 49.44°, and 53.19°, corresponding to the crystallographic planes of (002), (211), (112), (300), (202), (310), (222), (213), and (311) of $Ca_{10}(PO_4)_6(OH)_2$, respectively (JCPDS No: 01-074-0565). respectively. By using equation 1, the nHA crystal size was estimated to be ~40 nm in the (112)

direction. Furthermore, the strong and sharp peaks imply that nHA possesses a good crystalline degree.

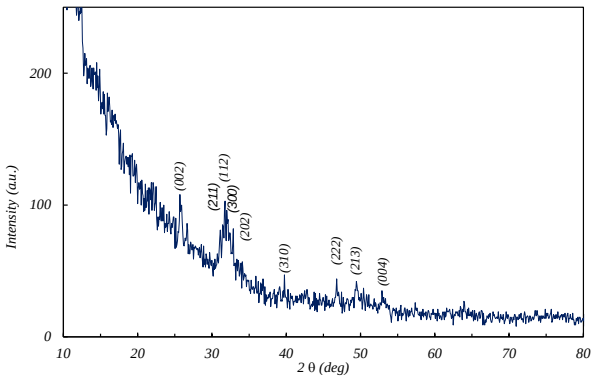

Figure 1. (**A**) X-ray diffraction patterns (XRD) of nHA.

UV-Vis absorption measurements

To offer evidence for the formation of the fibrillar BLG-Mumijo-nHA complex, UV-Vis spectroscopy measurements were carried out. As demonstrated in Fig. 2, native BLG has two strong absorption bands (λ_{max}): ~208 nm and ~278 nm. The absorption band at ~208 nm is assigned to the $n \rightarrow \pi^*$ transition of $C=O$ in the BLG backbone, i.e., the λ_{max} at 208 nm indicates the BLG framework structure (Zhao et al., 2010; Lu et al., 2016). The λ_{max} at around 278 nm in the BLG spectrum is attributed to the $\pi \rightarrow \pi^*$ transition of aromatic residues and is dependent on the micro-environment wherein the aromatic residues are located (Lu et al., 2016). As displayed in Fig. 2, adjustment of BLG at pH 2 and then incubation at 343 K made an increment in the λ_{max} at 278 nm. This enhancement is indeed attributable to the disorders in the micro-environment of BLG. Furthermore, the absorption spectra revealed that more side chains of aromatic residues of BLG were exposed to the solvent (Hao et al., 2016). The enhancement in the λ_{max} at 208 nm also signifies that the BLG framework structure changed. Frequently, by increasing the temperature, the hydrogen bonds in the protein are weakened; even though the hydrophobic interactions are activated and strengthened the aggregation process. It was revealed that peptides, and not the intact monomers, are the building blocks of the fibrils derived from BLG heated at 353 K and pH 2. Hence, BLG has to be hydrolyzed first, and then fibril formation can occur (Akkermans et al., 2008; Mazaheri et al., 2015). The UV-Visible spectrum of Mumijo is shown in Fig. 2. The sample did not demonstrate any sharp maxima which could be owing to the multi-component nature of Mumijo with a number of chromophores that have different absorbances (Agarwal et al., 2008). In addition, there was no obvious λ_{max} for nHA. Our observation correlates with those of Ion *et al.* (Ion et al., 2018). The UV-Visible spectrum of the fibrillar BLG-Mumijo-nHA solution displayed a reduction in the λ_{max} at both 208 and 278 nm. This phenomenon could be assigned to the formation of a complex between fibrillar BLG, Mumijo, and nHA.

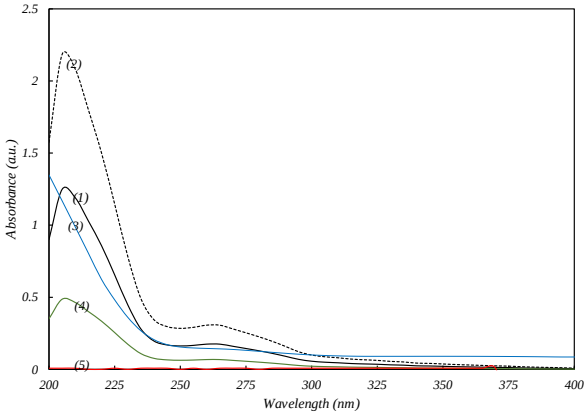

Figure 2. The UV-Visible spectra of native BLG solution (1), fibrillar BLG (2), Mumijo (3), fibrillar BLG-Mumijo-nHA complex (4), and nHA (5) at 310 K.

Steady-state fluorescence measurements

Fluorescence spectroscopy is one of the most effective methods to evaluate the structure and properties of bio-macromolecules. Therefore, the formation of a complex between BLG, Mumijo, and nHA was evaluated using the fluorescence method. Earlier studies have demonstrated that a BLG monomer contains two tryptophan residues (Trp_{19} and Trp_{61}) and four tyrosine residues (Tyr_{20}, Tyr_{42}, Tyr_{99}, and Tyr_{101}), which can possess intrinsic fluorescence. It is worth noting that, the intrinsic fluorescence property of BLG is almost exclusively due to the Trp_{19} residue because Trp_{61} is partly exposed to an aqueous solvent while Trp_{19} is located in an apolar environment (Pal et al., 2020; Wang et al., 2021). As shown in Fig. 3, BLG has a maximum intensity ($\lambda_{max,em}$) of about 332 nm. However, after adjustment of BLG at pH 2 and then incubation at 343 K a significant enhancement in the fluorescence emission with a slight red shift was observed. This phenomenon reflected considerable enhancement of the accessibility of the Trp_{19} moiety of BLG to the solvent (Pal et al., 2020). However, after the addition of Mumijo and nHA

a great reduction in the fluorescence of fibrillar BLG was detected. A reduction in fluorescence intensity could be attributable to the variation in polarity of microenvironments around the Trp moieties in the presence of Mumijo and nHA. This phenomenon could be assigned to the formation of a complex between fibrillar BLG, Mumijo, and nHA. It should be noted that Mumijo and nHA had no fluorescence emission (Pal et al. 2020).

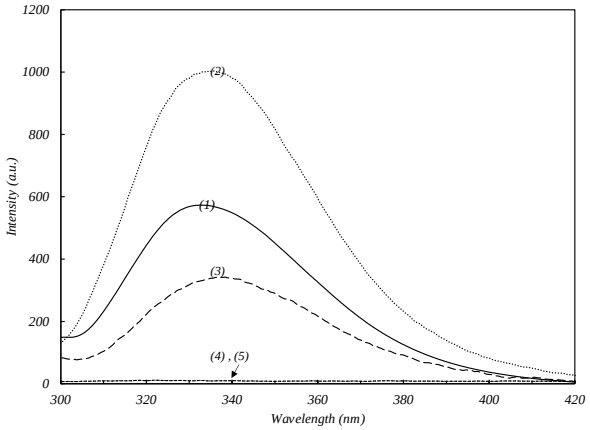

Figure 3. The fluorescence emission spectra of native BLG solution (1), fibrillar BLG (2), fibrillar BLG-Mumijo-nHA complex (3), Mumijo (4), and nHA (5) at 310 K.

Far-UV CD measurements

CD spectroscopy can determine any alternation in the secondary/tertiary structure of biomacromolecules, typically proteins. As displayed in Fig. 4, the far-UV CD spectrum of BLG was detected via the presence of a remarkable negative band at ~217 nm wavelength. Consequently, the content of the BLG secondary structure was analyzed. BLG consists of 19.90% α-helix, 52.70% β-sheet, and 27.40% random coil (Table 1). Consequently, BLG is primarily a β-structure protein. Our observation is coincident with those published by Pal *et. al*. (Pal et al., 2020) and Wang *et. al*. (Wang et al., 2021). Compared with the native BLG, far-UV CD studies of BLG subjected to pH 2 and then incubation at 343 K demonstrated a significant shift of the band position. Obviously, the secondary structure of fibrillar BLG was changed, i.e., the α-helix content increased slightly (20.10%), the contents of the β-sheet decreased (45.47%) and at the same time, the content of the random coil structure increased (34.60%). nHA had no far-UV CD signal in the 195-260 nm spectral region and Mumijo displayed noisy CD spectra in this region. After the addition of Mumijo and nHA to the fibrillar BLG solution, lots of negative bands were observed. The disappearance of the exact band near 205 nm, demonstrates the formation of a complex between fibrillar BLG, Mumijo, and nHA. This observation reveals good agreement with fluorescence emission as well as UV-Vis absorption data as mentioned above. It was confirmed that at pH 2 BLG has a monomeric structure and at neutral pH has a dimeric state. In strongly acidic conditions, BLG chains are extremely positively charged, and they repel each other, while in neutral pH conditions, the dimeric state is stabilized thru hydrogen bonds between the anti-parallel β-sheet and the surface AB loop (Gołębiowski et al., 2020). Thus, it could be possible that fibrillar BLG could bind with Mumijo by ionic interactions.

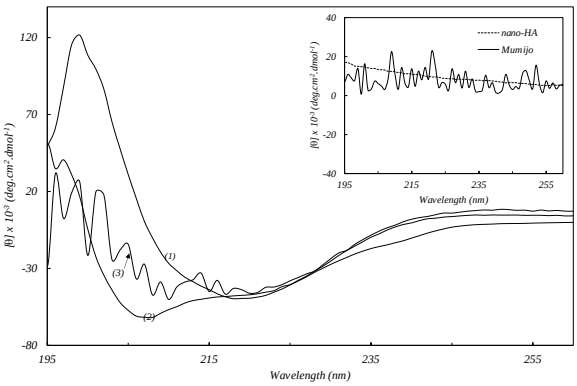

Figure 4. The far-UV CD spectra of native BLG solution (1), fibrillar BLG (2), and fibrillar BLG-Mumijo-nHA complex (3) at 310 K. Insert: the far-UV CD spectra of Mumijo and nHA.

Table 1. Content of the secondary structure of BLG, fibrillar BLG, and fibrillar BLG-Mumijo-nHA complex at 310 K.

	α-helix (%)	β-sheet (%)	Random coil (%)
BLG	19.90	52.70	27.40
fibrillar BLG	20.10	45.47	34.60
fibrillar BLG-Mumijo-nHA complex	15.63	47.67	36.72

FTIR measurements

FTIR spectroscopy was utilized to clarify the functional groups of the fibrillar BLG-Mumijo-nHA complex. In the FT-IR spectrum of BLG (Fig. 5A), the presence of the peak at the wavenumbers of 1644.6 and 1527.8 cm^{-1}

is associated with the amid I and amid II of protein, respectively. The presence of the peaks at the wavenumber between 3300-3500 cm^{-1} is related to the OH group. After adjustment of BLG to pH 2 and then incubation at 343 K, peaks at the wavenumbers between 1600-1700 cm^{-1} disappeared (Fig. 5B). Furthermore, peaks at the wavenumbers between 1500-1600 cm^{-1} disappeared. Thus, it seems that fibrillar BLG lost its structure. Fig. 4C displays the FTIR spectrum of the nHA. The peak at 3785.6 cm^{-1} corresponds to the stretching vibration of OH^{-1} ion in the nHA lattice. The peaks at 3180.4 cm^{-1} and 3466.3 cm^{-1} are related to the OH^{-1} ion and absorbed water, respectively. The peaks between 1400-1600 cm^{-1} are attributed to carbonates. Peaks at 607 cm^{-1} and 565.8 cm^{-1} are derived from ν_4 bending vibrations of P-O mode. The peak at 960.7 cm^{-1} resulted from the ν_1 symmetric P-O stretching vibrations (Gheisari et al., 2015; Mujahid et al., 2015). Fig. 4D reveals the FTIR spectrum of Mumijo. The peak at 3405.25 cm^{-1} is related to the free or bonded OH group which is related to the presence of phenols, polyphenols, and tannins. A peak between 2000-3000 cm^{-1} is related to the stretching vibration of alkanes and asymmetric stretching vibrations of the CH group of carbohydrate tail in Mumijo. The peak at 1403.99 cm^{-1} is related to bending vibrations of OH in alcohols and carboxylic acid. The peak at 1621.17 cm^{-1} is related to the carboxyl-derived NH_2 (amide) bond. The peak at 1051.34 cm^{-1} is related to the stretching vibrations of OH-CH in sugar and polysaccharides (Reddy, 2017; Hadi et al., 2020; Norouzi et al., 2020). In the FT-IR spectrum of the fibrillar BLG-Mumijo-nHA complex (Fig. 4E), a peak at 3416 cm^{-1} which is related to the OH groups of the BLG and Mumijo could be observed. The peak at t 1418.69 cm^{-1} is related to the bending vibrations of OH in Mumijo. The peak at 1647.20 cm^{-1} can be related to the carbonate group of nHA. Thus, it seems that a complex between fibrillar BLG, Mumijo, and nHA was formed.

Characterization of fibrillar BLG-Mumijo-nHA complex

SEM has a unique ability to evaluate the surface morphology of materials. Thus, the morphology of the fibrillar BLG-Mumijo-nHA complex was investigated using SEM. It can be realized from the images revealed in Fig. 6A and B that there is a difference in Mumijo structure before and after the addition of fibrillar BLG and nHA and the surface of Mumijo became rough. The image reveals that a layer of the fibrillar BLG-Mumijo-nHA complex was created. The zeta (ζ) potential is a particle's surface electrical charge measurement (Ghosh et al., 2014). The ζ-potential of the fibrillar BLG-Mumijo-nHA complex was found to be -12.6 mV. It has been reported that ζ-potential values of ±20-30 mV are related to moderately stable materials (Bhattacharjee, 2016). Consequently, it could be concluded that the fibrillar BLG-Mumijo-nHA complex is moderately stable.

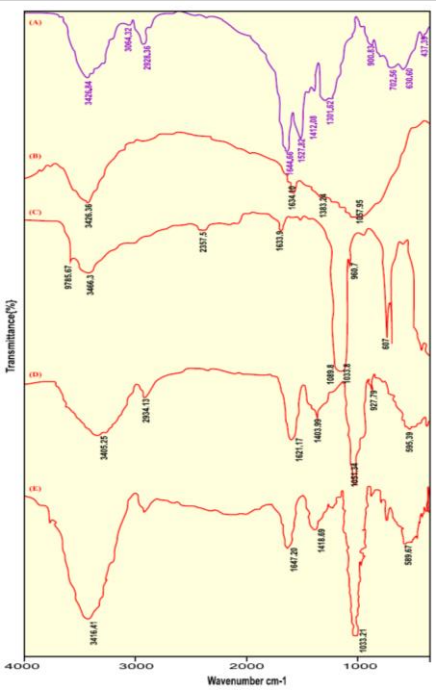

Figure 5. The FTIR spectra of native BLG solution (A), fibrillar BLG (B), nHA (C), Mumijo (D), and fibrillar BLG-Mumijo-nHA complex (E) at 310 K.

Growth rates of rBMMSCs by MTT assay

Since the cytotoxicity test of a novel material is the first-level evaluation before biomedical applications, we have performed *in vitro* assays to determine the effects exerted by fibrillar BLG-Mumijo-nHA complex on rBMMSCs growth. As seen in Fig. 7, the fibrillar BLG-Mumijo-nHA complex increased the viability of rBMMSCs in comparison with the control group at higher concentrations ($p \leq 0.05$). In other words, the fibrillar BLG-Mumijo-nHA complex has a positive influence on rBMMSCs growth. Thus, although more investigation must be done, the fibrillar BLG-Mumijo-

nHA complex could be a good candidate for bone regeneration.

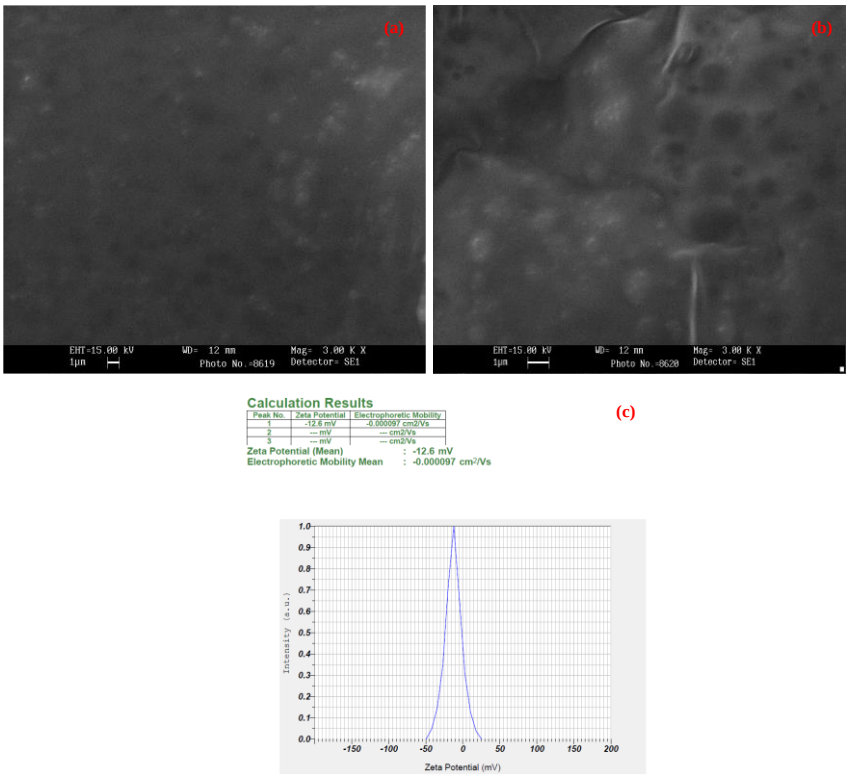

Figure 6. The SEM images of Mumijo (a) and the fibrillar BLG-Mumijo-nHA complex (b). The zeta potential measurement of the fibrillar BLG-Mumijo-nHA complex (c).

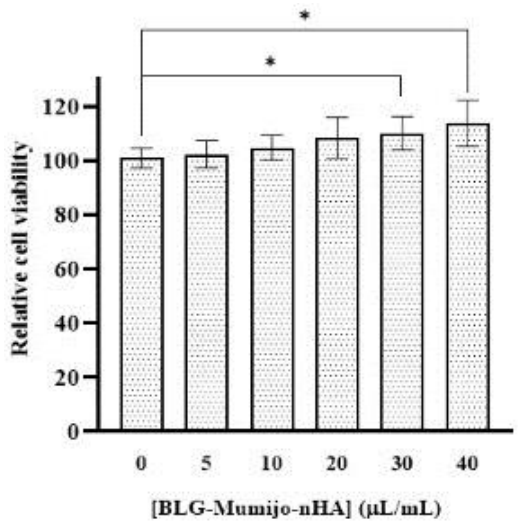

Figure 7. MTT assay of rBMMSCs after treatment with fibrillar BLG-Mumijo-nHA complex. Values are mean ± standard deviation; * indicates $P<0.05$.

Conclusion

Numerous recent articles describe state-of-art bone regeneration utilizing natural products, nanomaterials, and even biopolymers. In this study, we synthesized and introduced the fibrillar BLG-Mumijo-nHA complex in detail. By utilizing UV-Visible, fluorescence emission, and CD spectroscopy the formation of a complex was confirmed. Furthermore, the image and ζ-potential value of the fibrillar BLG-Mumijo-nHA complex were investigated. Furthermore, the complex has a positive impact on rBMMSCs growth. Accordingly, although further experiments are warranted to draw firm conclusions, we can propose that the fibrillar BLG-Mumijo-nHA complex could be a good candidate for the treatment of osteoporosis and bone fractures.

Ethical Statement

The study was approved by the Research Ethics Committees of Islamic Azad University- Science and Research Branch, Tehran, Iran (approval code: IR.IAU.SRB.REC.1400.396). This article does not

contain any studies with human participants or animals performed by any of the authors.

Competing Interests

The authors declare no conflict of interest.

Funding

No funding was received for this research article.

Authors Contribution

Negar Khiabani performed the lab experiments. Negar Khiabani and Azadeh Hekmat conceived the study, designed the experiments, and wrote the manuscript. Aghdas Banaei co-supervised the project. Azadeh Hekmat supervised the research and conceived the original idea. All authors read and approved the final version of the manuscript.

References

Abbasi, N., Azizpour, Y., Azizi, M., Karimi, E., Aidy, A. and K. Asadollahi, (2019). "The effects of mumie extract on cell proliferation and enzyme expression of human osteoblast-like cells (MG63)." *Journal of Stem Cells & Regenerative Medicine*, **15**(2): 18-23. DOI: https://doi.org/10.46582/jsrm.1502006.

Agarwal, S. P., Khanna, R., Karmarkar, R., Anwer, M. K. and R. K. Khar, (2008). "Physico-chemical, spectral and thermal characterization of Shilajit, a humic substance with medicinal properties." *Asian Journal of Chemistry*, **20**(1): 209-217. DOI: https://doi.org/10.2298/JSC1000006A.

Aiello, A., Fattorusso, E., Menna, M., Vitalone, R., Schröder, H. C. and W. E. Müller, (2011). "Mumijo traditional medicine: fossil deposits from antarctica (chemical composition and beneficial bioactivity)." *Evidence-Based Complementary and Alternative Medicine*, **2011**. 738131. DOI: https://doi.org/10.1093/ecam/nen072.

Akkermans, C., Venema, P., van der Goot, A. J., Gruppen, H., Bakx, E. J., Boom, R. M. and E. van der Linden, (2008). "Peptides are building blocks of heat-induced fibrillar protein aggregates of β-lactoglobulin formed at pH 2." *Biomacromolecules*, **9**(5): 1474-1479. DOI: https://doi.org/10.1021/bm7014224.

Arpornmaeklong, P., Jaiman, N., Apinyauppatham, K., Fuongfuchat, A. and S. Boonyuen, (2023). "Effects of calcium carbonate microcapsules and nanohydroxyapatite on properties of thermosensitive chitosan/collagen hydrogels". *Polymers*, **15**(2): 416. DOI: https://doi.org/10.3390/polym15020416.

Bhattacharjee, P., Kundu, B., Naskar, D., Kim, H.-W., Maiti, T. K., Bhattacharya, D. and S. C. Kundu, (2017). "Silk scaffolds in bone tissue engineering: An overview." *Acta Biomaterialia*, **63**: 1-17. DOI: https://doi.org/10.1016/j.actbio.2017.09.027.

Bhattacharjee, S. (2016). "DLS and zeta potential–what they are and what they are not?" *Journal of Controlled Release*, **235**: 337-351. DOI: https://doi.org/10.1016/j.jconrel.2016.06.017.

Bolisetty, S., Peydayesh, M. and R. Mezzenga, (2019). "Sustainable technologies for water purification from heavy metals: review and analysis." *Chemical Society Reviews*, **48**(2): 463-487. DOI: https://doi.org/10.1039/C8CS00493E.

Cao, Y. and R. Mezzenga, (2019). "Food protein amyloid fibrils: Origin, structure, formation, characterization, applications and health implications." *Advances in Colloid and Interface Science*, **269**: 334-356. DOI: https://doi.org/10.1016/j.cis.2019.05.002.

Cesur, M. G., Ogrenim, G., Gulle, K., Sirin, F. B., Akpolat, M. and G. Cesur, (2019). "Does shilajit have an effect on new bone remodelling in the rapid maxillary expansion treatment? a biochemical, histopathological and immunohistochemical study." *SDÜ Tıp Fakültesi Dergisi*, **26**(1): 96-103. DOI: https://doi.org/10.17343/sdutfd.511364.

Ding, R., Zhao, M., Fan, J., Hu, X., Wang, M., Zhong, S. and R. Gu, (2020). "Mechanisms of generation and exudation of Tibetan medicine Shilajit (Zhaxun)." *Chinese Medicine*, **15**(1): 1-15. DOI: https://doi.org/10.1186/s13020-020-00343-9.

Douglas, T. E., Vandrovcová, M., Kročilová, N., Keppler, J. K., Zárubová, J., Skirtach, A. G. and L. Bačáková, (2018). "Application of whey protein isolate in bone regeneration: Effects on growth and osteogenic differentiation of bone-forming cells." *Journal of Dairy Science*, **101**(1): 28-36. DOI: https://doi.org/10.3168/jds.2017-13119.

Dufour, E., Roger, P. and T. Haertlé, (1992). "Binding of benzo (α) pyrene, ellipticine, and cis-parinaric acid to β-lactoglobulin: Influence of protein modifications." *Journal of Protein Chemistry*, **11**: 645-652. DOI: https://doi.org/10.1007/BF01024965.

Gheisari, H., Karamian, E. and M. Abdellahi, (2015). "A novel hydroxyapatite–Hardystonite nanocomposite ceramic." *Ceramics International*, **41**(4): 5967-5975. DOI: https://doi.org/10.1016/j.ceramint.2015.01.033.

Ghosh, D., Dey, S. K. and C. Saha, (2014). "Mutation induced conformational changes in genomic DNA from cancerous K562 cells influence drug-DNA binding modes." *PloS One*, **9**(1): e84880. DOI: https://doi.org/10.1371/journal.pone.0084880.

Gołębiowski, A., Pomastowski, P., Rodzik, A., Król-Górniak, A., Kowalkowski, T., Górecki, M. and B. Buszewski, (2020). "Isolation and self-association studies of beta-lactoglobulin." *International Journal of Molecular Sciences*, **21**(24): 9711. DOI: https://doi.org/10.3390/ijms21249711.

Hadi, S., Ahmed, S. H., Talib, N., Hussein, H. A. and I. H. T. Al-Karkhi, (2020). "Alcoholic extract of shilajit as anti protein denaturation, anti blood hemolysis, and anti microbial." *Indian Journal of Forensic Medicine & Toxicology*, **14**(1): 392-396. DOI: https://doi.org/10.37506/ijfmt.v14i1.77.

Hao, M. and R. Liu, (2016). "Influence of mercaptopropionic-acid-capped CdTe quantum dots on the human chorionic gonadotropin structure and activity alterations." *RSC Advances*, **6**(84): 80383-80389. DOI: https://doi.org/10.1039/C6RA12199C.

Hekmat, A., Salavati, F. and S. H. Tackallou, (2020). "The effects of paclitaxel in the combination of diamond nanoparticles on the structure of human serum albumin (HSA) and their antiproliferative role on MDA-MB-231cells." *The Protein Journal*: **39**(3): 268-283. DOI: https://doi.org/10.1007/s10930-020-09882-4.

Hekmat, A., Saso, L., Lather, V., Pandita, D., Kostova, I. and A. A. Saboury, (2022) "Recent advances in nanomaterials of group XIV elements of periodic table in breast cancer treatment." *Pharmaceutics*, **14**(12): 2640. DOI: https://doi.org/10.3390/pharmaceutics14122640.

Ion, R.-M., Nyokong, T., Nwahara, N., Suica-Bunghez, I.-R., Iancu, L., Teodorescu, S., Dulama, I. D., Stirbescu, R. M., Gheboianu, A. and R. M. Grigorescu, (2018). "Wood preservation with gold hydroxyapatite system." *Heritage Science*, **6**(1): 1-12. DOI: https://doi.org/10.1186/s40494-018-0202-5.

Islam, M. S., Ebrahimi-Barough, S., Al Mahtab, M., Shirian, S., Aghayan, H. R., Arjmand, B., Allahverdi, A., Ranjbar, F. E., Sadeg, A. B. and J. Ai, (2022). "Encapsulation of rat bone marrow-derived mesenchymal stem cells (rBMMSCs) in collagen type I containing platelet-rich plasma for osteoarthritis treatment in rat model." *Progress in Biomaterials*, **11**(4): 385-396. DOI: https://doi.org/10.1007/s40204-022-00200-y.

Jang, J. H., Kim, S., Lee, H. J., Suh, H. J. and K. Jo, (2021). "Stimulating effect of whey protein hydrolysate on bone growth in MC3T3-E1 cells and a rat model." *Food & Function*, **12**(11): 5109-5117. DOI: https://doi.org/10.1039/D1FO00546D.

Keppler, J. K., Heyn, T. R., Meissner, P. M., Schrader, K. and K. Schwarz, (2019). "Protein oxidation during temperature-induced amyloid aggregation of beta-lactoglobulin." *Food Chemistry*, **289**: 223-231. DOI: https://doi.org/10.1016/j.foodchem.2019.02.114.

Kim, Y. E., Kim, J. W., Cheon, S., Nam, M. S. and K. K. Kim, (2019). "Alpha- Casein and beta- lactoglobulin from cow milk exhibit antioxidant activity: a plausible link to antiaging effects." *Journal of Food Science*, **84**(11): 3083-3090. DOI: https://doi.org/10.1111/1750-3841.14812.

Kloskowski, T., Szeliski, K., Krzeszowiak, K., Fekner, Z., Kazimierski, Ł., Jundziłł, A., Drewa, T. and M. Pokrywczyńska, (2021). "Mumio (Shilajit) as a potential chemotherapeutic for the urinary bladder cancer treatment." *Scientific Reports*, **11**(1): 1-12. DOI: https://doi.org/10.1038/s41598-021-01996-8.

Lu, Q., Chen, C., Zhao, S., Ge, F. and D. Liu, (2016). "Investigation of the interaction between gallic Acid and α-amylase by spectroscopy." *International Journal of Food Properties*, **19**(11): 2481-2494. DOI: https://doi.org/10.1080/10942912.2015.1059345.

Mazaheri, M., Moosavi-Movahedi, A. A., Saboury, A. A., Khodagholi, F., Shaerzadeh, F. and N. Sheibani, (2015). "Curcumin protects β-lactoglobulin fibril formation and fibril-induced neurotoxicity in PC12cells." *PLoS One*, **10**(7): e0133206. DOI: https://doi.org/10.1080/10942912.2015.1059345.

Meimandi-Parizi, A., Oryan, A. and H. Gholipour, (2018). "Healing potential of nanohydroxyapatite, gelatin, and fibrin-platelet glue combination as tissue engineered scaffolds in radial bone defects of rats." *Connective Tissue Research*, **59**(4): 332-344. DOI: DOI: https://doi.org/10.1080/03008207.2017.1387541.

Mercadante, D., Melton, L. D., Norris, G. E., Loo, T. S., Williams, M. A., Dobson, R. C. and G. B. Jameson, (2012). "Bovine β-lactoglobulin is dimeric under imitative physiological conditions: dissociation equilibrium and rate constants over the pH range of 2.5–7.5." *Biophysical Journal*, **103**(2): 303-312. DOI: https://doi.org/10.1016/j.bpj.2012.05.041.

Mishra, T., Dhaliwal, H. S., Singh, K. and N. Singh, (2019). "Shilajit (Mumie): current status of biochemical, therapeutic and clinical advances." *Current Nutrition & Food Science*, **15**(2): 104-120. DOI: https://doi.org/10.2174/1573401313666170823160217.

Mohammad-Beigi, H., Wijaya, W., Madsen, M., Hayashi, Y., Li, R., Rovers, T. A. M., Jæger, T. C., Buell, A. K., Hougaard, A. B. and J. J. Kirkensgaard, (2023). "Association of caseins with β-lactoglobulin influenced by temperature and calcium ions: A multi-parameter analysis." *Food Hydrocolloids*, **137**: 108373. DOI: https://doi.org/10.1016/j.foodhyd.2022.108373.

Mujahid, M., Sarfraz, S. and S. Amin, (2015). "On the formation of hydroxyapatite nano crystals prepared using cationic surfactant." *Materials Research*, **18**: 468-472. DOI: https://doi.org/10.1590/1516-1439.298014.

Noori, A., Ashrafi, S. J., Vaez-Ghaemi, R., Hatamian-Zaremi, A. and T. J. Webster, (2017). "A review of fibrin and fibrin composites for bone tissue engineering." *International Journal of Nanomedicine*, **12**: 4937. DOI: https://doi.org/10.2147/IJN.S124671.

Norouzi, F. and S. Javanshir, (2020). "Magnetic γFe_2O_3@ Sh@ Cu_2O: an efficient solid-phase catalyst for reducing agent and base-free click synthesis of 1, 4-disubstituted-1, 2, 3-triazoles." *BMC Chemistry*, **14**(1): 1-16. DOI: https://doi.org/10.1186/s13065-019-0657-9.

Pal, S., Maity, S., Sardar, S., Begum, S., Dalui, R., Parvej, H., Bera, K., Pradhan, A., Sepay, N. and S. Paul, (2020). "Antioxidant ferulic acid prevents the aggregation of bovine b-lactoglobulin *in vitro*." *Journal of Chemical Sciences*, **132**:103. DOI: https://doi.org/10.1007/s12039-020-01796-z.

Pingali, U. and C. Nutalapati, (2022). "Shilajit extract reduces oxidative stress, inflammation, and bone loss to dose-dependently preserve bone mineral density in postmenopausal women with osteopenia: A randomized, double-blind, placebo-controlled trial." *Phytomedicine*, **105**: 154334. DOI: https://doi.org/10.1016/j.phymed.2022.154334.

Reddy, K. (2017). "Analytical substantiation of an antidiabetic ayurvedic formulation eladi churna through fourier transmission infrared." *Asian Journal of Pharmaceutics (AJP)*, **11**(04): 1298-1301. DOI: https://doi.org/10.22377/ajp.v11i04.1626.

Saber-Samandari, S., Saber-Samandari, S., Ghonjizade-Samani, F., Aghazadeh, J. and A. Sadeghi, (2016). "Bioactivity evaluation of novel nanocomposite scaffolds for bone tissue engineering: The impact of hydroxyapatite." *Ceramics International*, **42**(9): 11055-11062. DOI: https://doi.org/10.1016/j.ceramint.2016.04.002.

Sadeghinia, A., Davaran, S., Salehi, R. and Z. Jamalpoor, (2019). "Nano-hydroxy apatite/chitosan/gelatin scaffolds enriched by a combination of platelet-rich plasma and fibrin glue enhance proliferation and differentiation of seeded human dental pulp stem cells." *Biomedicine & Pharmacotherapy*, **109**: 1924-1931. DOI: https://doi.org/10.1016/j.biopha.2018.11.072.

Saini, P., Sharma, R. and N. Chadha, (2017). "Determination of defect density, crystallite size and number of graphene layers in graphene analogues using X-ray diffraction and Raman spectroscopy." *Indian Journal of Pure & Applied Physics (IJPAP)*, **55**(9): 625-629. DOI: 10.56042/ijpap.v55i9.16047.

Saxena, V. and L. M. Pandey, (2021). "Synthesis and sintering of calcium hydroxyapatite for biomedical applications." *Journal of Materials Science: Materials in Medicine*, **17**: 1063–1068. DOI: https://doi.org/10.1007/s10856-006-0532-9.

Wang, Y., Gong, M., Huang, Z., Min, H., Yu, P., Tang, F., Ye, Y., Zhu, S., Hu, Z. and Z. Zeng, (2021). "Spectroscopic and theoretical investigation of β-Lactoglobulin interactions with hematoporphyrin and protoporphyrin IX." *ACS Omega*, **6**(14): 9680-9691. DOI: https://doi.org/10.1021/acsomega.1c00279.

Wei, G., Su, Z., Reynolds, N. P., Arosio, P., Hamley, I. W., Gazit, E. and R. Mezzenga, (2017). "Self-assembling peptide and protein amyloids: from structure to tailored function in nanotechnology." *Chemical Society Reviews*, **46**(15): 4661-4708. DOI: https://doi.org/10.1039/C6CS00542J.

Zhao, X., Liu, R., Chi, Z., Teng, Y. and P. Qin, (2010). "New insights into the behavior of bovine serum albumin adsorbed onto carbon nanotubes: comprehensive spectroscopic studies." *The Journal of Physical Chemistry B*, **114**(16): 5625-5631. DOI: https://doi.org/10.1021/jp100903x.

Zhao, Z.-h., Ma, X.-l., Ma, J.-x., Kang, J.-y., Zhang, Y. and Y. Guo, (2022). "Sustained release of naringin from silk-fibroin-nanohydroxyapatite scaffold for the enhancement of bone regeneration." *Materials Today Bio*, **13**: 100206. DOI: https://doi.org/10.1016/j.mtbio.2022.100206.

